Available online at www.sciencedirect.com
ScienceDirect
Advances in Space Research 47 (2011) 2081–2091
ADVANCES IN SPACE RESEARCH (a COSPAR publication)
www.elsevier.com/locate/asr

Actors of the main activity in large complex centres during the 23 solar cycle maximum

B. Schmieder [a,*], P. Démoulin [a], E. Pariat [a], T. Török [a,1], G. Molodij [a], C.H. Mandrini [b], S. Dasso [b], R. Chandra [c], W. Uddin [d], P. Kumar [d], P.K. Manoharan [e], P. Venkatakrishnan [f], N. Srivastava [f]

[a] Observatoire de Paris, LESIA, 92195 Meudon, France
[b] Instituto de Astronomía y Física del Espacio (UBA-CONICET) and Facultad de Ciencias Exactas y Naturales (UBA), Buenos Aires, Argentina
[c] Department of Physics, DSB Campus, Kumaun University, Nainital 263 002, Uttarakhand, India
[d] ARIES, Manora Peak, Nainital 263 129, India
[e] Radio Astronomy Centre, Tata Institute of Fundamental research, Udhagamandalam (Ooty) 643 001, India
[f] Udaipur Solar Observatory, P.O. Box, 198, Dewali, Udaipur 313 001, India

Available online 25 February 2011

Abstract

During the maximum of Solar Cycle 23, large active regions had a long life, spanning several solar rotations, and produced large numbers of X-class flares and CMEs, some of them associated to magnetic clouds (MCs). This is the case for the Halloween active regions in 2003. The most geoeffective MC of the cycle (Dst = −457) had its source during the disk passage of one of these active regions (NOAA 10501) on 18 November 2003. Such an activity was presumably due to continuous emerging magnetic flux that was observed during this passage. Moreover, the region exhibited a complex topology with multiple domains of different magnetic helicities. The complexity was observed to reach such unprecedented levels that a detailed multi-wavelength analysis is necessary to precisely identify the solar sources of CMEs and MCs. Magnetic clouds are identified using *in situ* measurements and interplanetary scintillation (IPS) data. Results from these two different sets of data are also compared.

Keywords: Active region; Coronal mass ejection; Magnetic clouds; Magnetic helicity

1. Introduction

Studies combining coronal and interplanetary observations allow us to link flares, filament eruptions and coronal mass ejections (CMEs) to interplanetary CMEs (ICMEs), including the subset called magnetic clouds (MCs). This kind of analysis allows us to follow the time evolution of the magnetic configuration from the Sun to interplanetary space, in particular to Earth. However, we still need a better understanding of the physics involved in order to better forecast Earth-directed events.

The solar and interplanetary data are of very different types and they give complementary informations. Solar data are remote sensing measurements but have a global nature. The results derived from the analysis of these observations are obtained after a complex analysis of spectral lines depending on calibration issues. These data provide a 2D view, and even a 3D view if multi-wavelength observations and/or magnetic field extrapolations are combined. In interplanetary space, the magnetized plasma can be studied using *in situ* measurements provided by spacecrafts, like the Magnetometer Instrument (MAG, Smith et al., 1998) aboard the Advanced Composition Explorer (ACE, Stone et al., 1998). Characteristics such as a smooth and large coherent rotation

* Corresponding author.
E-mail address: brigitte.schmieder@obspm.fr (B. Schmieder).
[1] Predictive Science, Inc., 9990 Mesa Rim Road San Diego, CA 92121, USA

0273-1177/$36.00 © 2011 COSPAR. Published by Elsevier Ltd. All rights reserved.
doi:10.1016/j.asr.2011.02.001

of the magnetic field vector, enhancements of the magnetic field intensity with respect to the surrounding solar wind, low proton temperature, and low plasma β indicate the presence of a MC (e.g., Burlaga et al., 1981; Dasso et al., 2007). *In situ* measurements have typically less calibration issues than remote sensing measurements, but they only provide data along a 1D cut through the structure crossed by the spacecraft. Then, models are used to derive a more global view such as a flux rope model fitted to the magnetic data of a MC. Another technique providing information of the structures travelling in interplanetary space uses the interplanetary scintillation (IPS) of radio sources (Manoharan, 2010). IPS observations of radio sources give the fluctuations in amplitude of radio waves from a distant compact radio source caused by density inhomogeneities in the solar wind. For example, important density inhomogeneities are created in the sheath formed in front of fast ICMEs (e.g., Bisi et al., 2010a, 2010b). Then, IPS measurements with a large number of radio sources on consecutive days provide the opportunity to track the propagation and expansion of CMEs from near the Sun to the Earth using a three dimensional reconstruction technique (see review of Jackson et al 2011) .

Several key steps can be followed to associate a CME to an ICME. The location of the activity on the Sun is the first one. An ICME is expected to be observed at the Earth vicinity if the flare or filament eruption is close to disk center (typically closer than a half solar radius from the disk center) or if a partial halo CME is observed. For such association we need to take into account the average angular width of CMEs $\sim$50° (St. Cyr et al., 2000) and non-radial motions (e.g., deflection by a streamer, Gopalswamy et al., 2000). There are also counter examples of eruptions close to the limb (Watari et al., 2001) or very large and global CMEs (Zhukov and Veselovsky, 2007) that produce effects on Earth. Furthermore, limb events can produce intense geomagnetic storms due to the large lateral extension of the ICME sheath (Gopalswamy et al., 2010).

The time between the solar event and its observation at 1 AU is a second criteria for an association. An ICME arrives at 1 AU between 1–5 days after the CME departure from the Sun. Information on the radial velocity permits to narrow this time interval. A backward extrapolation with constant velocity of the *in situ* data can be used to derive, which CME is responsible for the studied ICME. This is more accurate than starting from the Sun because *in situ* data provide the mean radial ICME velocity, as well as its expansion velocity (Démoulin, 2008). On the other hand the velocity of the CME is only determined by tracking its leading edge and it is typically difficult to correct for projection effects. Moreover, CME acceleration is dominantly present close to the Sun so that the mean travelling speed is difficult to estimate from the leading edge velocity. Another estimation of the travel time can be derived from interplanetary radio emission. Type II emissions complemented with an heliospheric density model allow us to track the ICME shock propagation (e.g., Hoang et al., 2007).

A third criteria for the association of a CME and an ICME or MC is the orientation of the magnetic flux rope which is commonly approximately conserved from the Sun to the Earth, apart of a rotation of a few 10° in the direction defined by the magnetic helicity sign (Green et al., 2007). A good relationship is statistically found between the MC axis direction and the filament orientation (Marubashi, 1997; Yurchyshyn et al., 2001, 2005, 2006). However, for some events a large rotation of the filament axis versus the associated MC axis is observed. This large rotation (writhing) of the axis, that can be as large as 70–140°, is a plausible clue for the kink instability (Fan and Gibson, 2003; Török and Kliem, 2005; Williams et al., 2005).

The magnetic helicity (H) is a well-conserved quantity in a given large-scale flux tube even with important magnetic energy release (Berger, 1984). The sign of H in an active region can be deduced from the spatial organization of the whorls around sunspots, filament fibrils and/or barbs, magnetic tongues in emerging ARs, shear of the flare loops along the photospheric inversion line (PIL), J-shaped flare ribbons, and/or X-ray sigmoids (see the review Démoulin and Pariat, 2009). The sign of H can also be derived from *in situ* magnetic field measurements, so the helicity sign is a fourth criteria for the association of a CME and a MC.

During the last Solar Cycle, in 2000, 2003, and 2005, huge complex active regions were particularly active. These active regions registered several X class flares during their disk passage and even 12 per day in 2005. The largest flare was identified as having X-ray class 21 on 4 November 2003. Also in 2003, we observed the famous series of flares called "Halloween events" and their associated MCs, e.g., AR NOAA 10486 flares on 28 October 2003 and its corresponding MC was detected on 29 October 2003 (Fig. 1, Schmieder et al., 2006; Mandrini et al., 2006; Dasso et al., 2006). During November 2003 several flares and their related CMEs were very geoeffective as extended MCs reached the Earth. The largest geomagnetic storm of the cycle, with Dst as low as -457 nT, has been related with the MC detected *in situ* on 20 November 2003.

The aim of this paper is to review the activity of a large complex active region and to determine the main actors responsible for this activity in the Sun–Earth system during the time period from 18 to 23 November 2003. Only a few studies cover the full chain of events from Sun to Earth (Dasso et al., 2009; Bisi et al., 2010a). Such studies are the basis for the prediction of active phenomena during the future solar maximum. We discuss in particular the ICMEs observed *in situ* by ACE and the IPS measurements that gives us clues on the characteristics of MCs.

2. Solar activity on 18 November and MC on 20 November 2003

Fig. 2 shows the temporal evolution of the flares observed by GOES on 18 November 2003. Seven flares of C to M class occurred during this day. Three of them

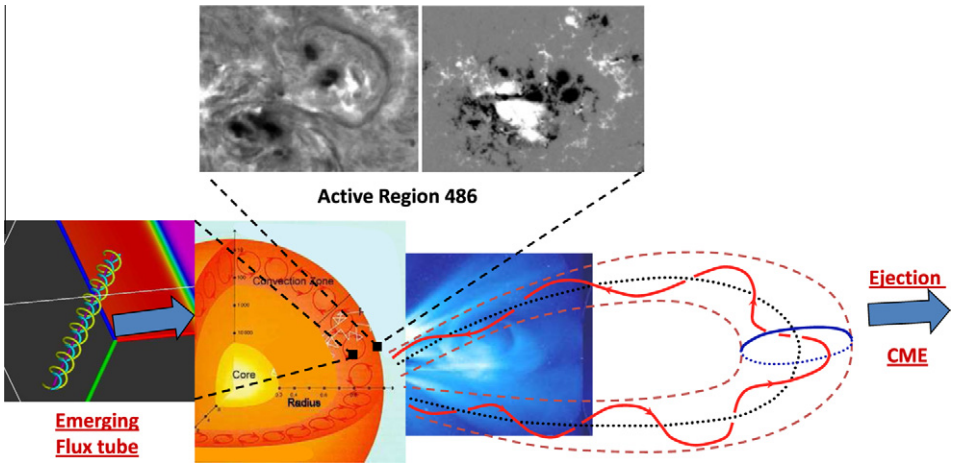

Fig. 1. (top right) Active region NOAA 10486 on 28 October 2003 observed in Hα during an X17 flare, one of the Halloween events (top left), and a longitudinal magnetogram of the same AR. (bottom) Sketch of an emerging flux tube crossing the convection zone and initiating a CME represented by a flux rope reaching the Earth. adapted from Démoulin (2008)

were observed to originate from AR 10501 (located at N03 E08). Their X-ray/Hα class are C3.8/SF at 05:25 UT, M3.2/2N at 07:52 UT, and M3.9/2N at 08:30 UT, respectively. These flares were associated with filament eruptions (Chandra et al., in press). The M3.2 and M3.9 flares have been associated with two CMEs, detected by the Large Angle and Spectrometric Coronagraph (LASCO, Brueckner et al., 1995). The first CME was detected in C2 field-of-view at 08:06 UT, it had a speed of $\sim$1220 km $\cdot$ s^{-1}, and a width of $\sim 100^{o}$. The second halo CME was observed at 08:50 UT with a speed of $\sim$1660 km $\cdot$ s^{-1}.

The MC associated to the 18 November 2003 solar active events extended from 11:16 UT to 18:44 UT on 20 November 2003 when observed at ACE (Möstl et al., 2008). In order to identify which of the filament ejections could be at the origin of this MC, we have proceeded doing backward extrapolation from the time the MC was observed to the corona using the *in situ* velocity measurements (see Introduction). The mean radial MC velocity observed by ACE was $\sim$600 km $\cdot$ s^{-1}. With a backward extrapolation to the corona, the solar ejection should have occurred 69 hours before. Taking $\sim$15:00 UT as the time for the MC center passing across ACE, the solar source event should have occurred at $\sim$18:00 UT on 17 November. The solar source can be searched taking a time window as long as $\pm$1 day, as used in some studies (Marubashi, 1997; Watari et al., 2001). Then, we searched from 16 November, 18:00 UT to 18 November 18:00 UT on the Sun. We found four CMEs on 17 November (*i.e.* at 08:50 UT, 09:26 UT, 13:50 UT, and 23:50 UT) and four CMEs on 18 November (*i.e.* at 05:26 UT, 08:06 UT, 08:50 UT, and 09:50 UT). It is generally believed that a MC will be observed in the Earth vicinity if its associated CME is a halo or a partial halo CME and if its source region is close

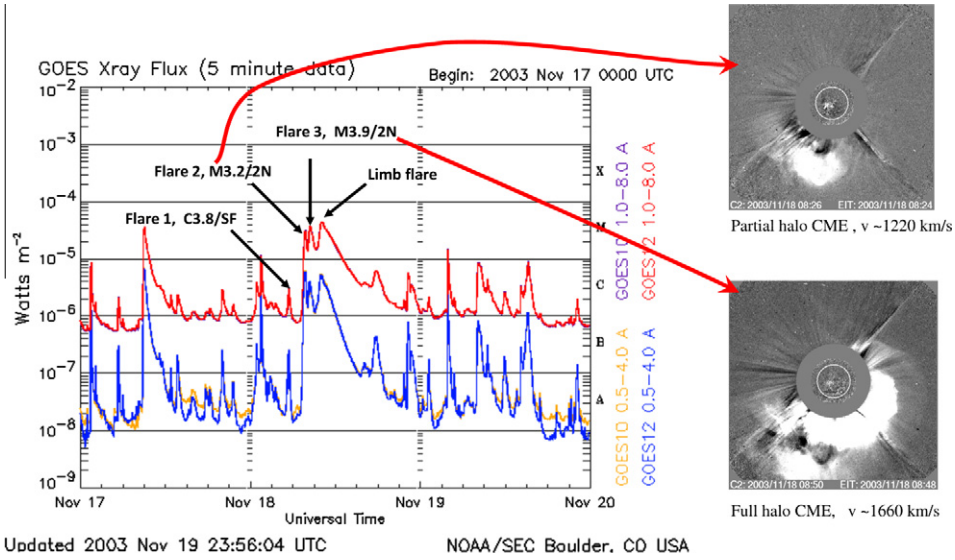

Fig. 2. (left panel) X-ray emission curves showing the two flares occurring on 18 November 2003, and (right panels) their corresponding CMEs observed with SOHO/LASCO C2 at 08:26 UT (top) and at 08:50 UT (bottom).

to the solar disk center (see Introduction). Therefore, as also proposed by Gopalswamy et al. (2005), the most probable solar source for the MC was the CME of 18 November 2003 at 08:50 UT. This is a halo CME that was associated with the largest flare and eruption from AR 10501, located close to solar disk center.

Different aspects of the MC of 20 November 2003, were studied by several authors (Yurchyshyn et al., 2005; Gopalswamy et al., 2005; Wang et al., 2006; Möstl et al., 2008); all of them concluded that the MC helicity was positive and that its source region was AR 10501. In particular, its magnetic helicity sign can be directly determined from *in situ* observations of the magnetic field (Fig. 3). In the classification of Bothmer and Schwenn (1994) this MC is an ESW cloud, which has a positive magnetic helicity.

3. Magnetic helicity injection in the active region

Fig. 4 shows the complex magnetic field of AR 10501 and Fig. 5 is a zoom of the region showing many bipoles on 18 November 2003. The two M class flares associated with the two CMEs occurred at a location marked by high magnetic field gradient which led to release of free energy stored in the active region (Srivastava et al., 2009). Nevertheless, the connectivity of positive/negative polarities can be derived using a linear force-free field extrapolation (Chandra et al., in press). The MDI movie indicates that

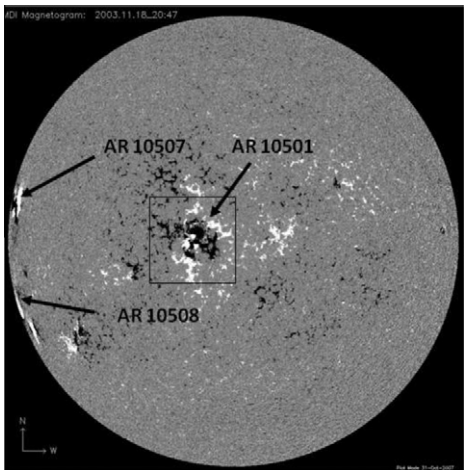

Fig. 4. Full disk longitudinal magnetic map (MDI) showing the complex magnetic field of AR 10501 on 18 November 2003 (positive/negative polarities are represented respectively in white/black). The box is the field-of-view of Fig. 5.

a new bipole (P3N3) starts emerging as the region arrives at the East limb. Polarity N3 rotates and breaks during its disk passage. The behavior of this emerging flux is the main actor of the activity in this AR and all the main flares have ribbons overlying this location.

From the analysis of various morphological features, fibrils, filaments and flare ribbons, (Chandra et al., 2010) conclude that the magnetic helicity is negative for AR

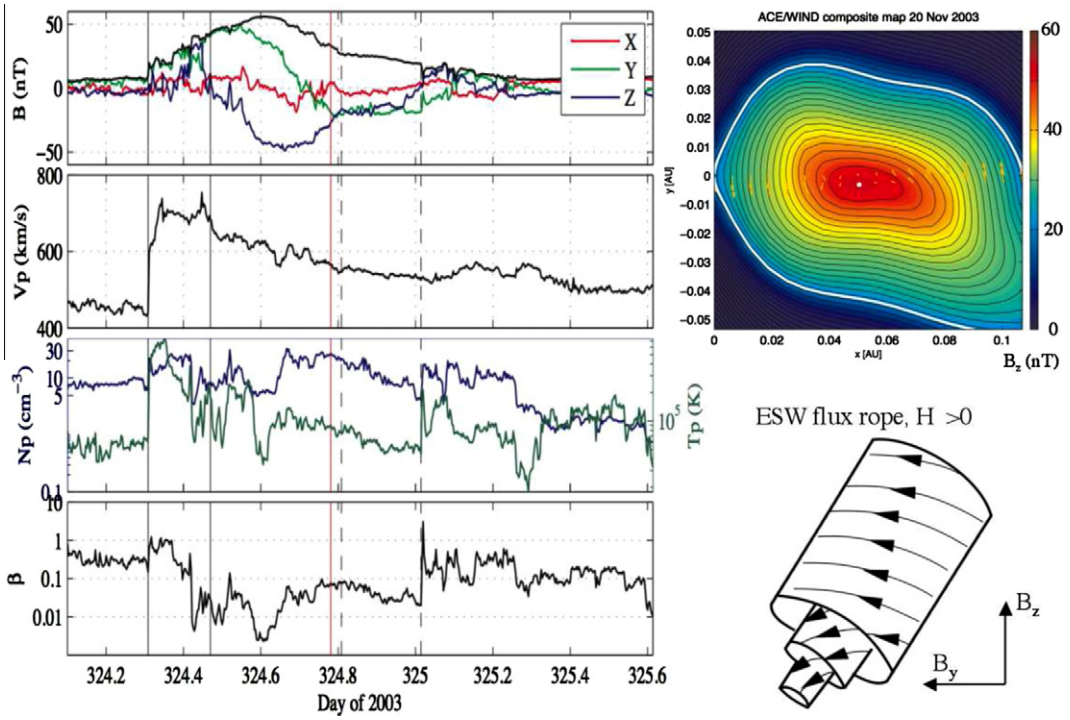

Fig. 3. (left panels) *In situ* observations of the MC on 20 November 2003 obtained by ACE showing the three components of the magnetic field, the velocity, the density and the plasma β. The x, y, z coordinates are in the Geocentric Solar Ecliptic (GSE) system. (top right) The cross-section of the flux rope, determined by integrating the Grad-Shafranov equation, with magnetic field lines representing the field (isocontours) in the x–y plane, the orthogonal field component is color coded with maximum at the center and points out of the paper. The arrows along the spacecraft trajectory are projections of the magnetic field vector onto the x–y plane (adapted from Möstl et al. (2008)). (bottom right) A sketch of the flux rope showing its orientation and helicity.

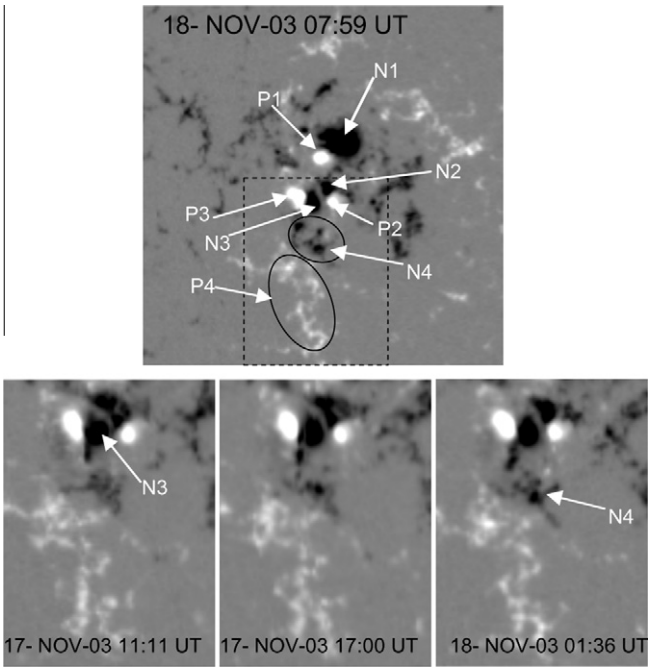

Fig. 5. Longitudinal magnetic field map of AR 10501 showing the multiple bipoles and their evolution versus time before the eruption. P3N3 is the emerging bipole. N3 rotates around P3 and breaks in many pieces pushing N4 towards the East. These motions induce a large shear along the magnetic inversion line where lies the erupting filament between N4,P4 (represented by the two ovales in the top panel). Positive/negative polarities are represented respectively in white/black. The size of the top image is 370″ × 370″, the dashed box represents the field-of-view of the lower panels (130″ × 200″).

10501. The magnetic tongues of the emerging bipole P3N3 also indicate the emergence of a flux rope with negative magnetic helicity. The magnetic tongues are the extensions of the magnetic polarities formed by the azimuthal field component of the flux rope (López Fuentes et al., 2000; Chandra et al., 2009). Then, all the solar proxies of helicity indicate an helicity sign opposite to the one of the associated MC (Fig. 3).

One can also derive the magnetic helicity flux at the photospheric level from the temporal series of magnetograms. The helicity flux dH/dt is computed by integrating over the AR the quantity called G_θ which is an approximation of the magnetic helicity flux per unit surface (Pariat et al., 2005). The helicity accumulation, ΔH, is determined by the time integration of the helicity flux:

$$\left.\frac{dH}{dt}\right|_{AR} = \int_{AR} G_\theta d^2x, \quad \Delta H = \int_{t_i}^{t_f} \left.\frac{dH}{dt}\right|_{AR} dt \qquad (1)$$

with t_i and t_f the initial and final times. The helicity accumulation profile presents two stages, first a global linear decrease of $|dH/dt|$ followed by a nearly constant dH/dt a few hours before the eruption and later on (Fig. 6). This decrease of $|dH/dt|$ was previously found in other ARs, in particular in intense flaring regions (Park et al., 2008).

Chandra et al. (2010) show that in the two days preceding the flares, more than -4×10^{26} Wb^2(-4×10^{42} Mx^2)

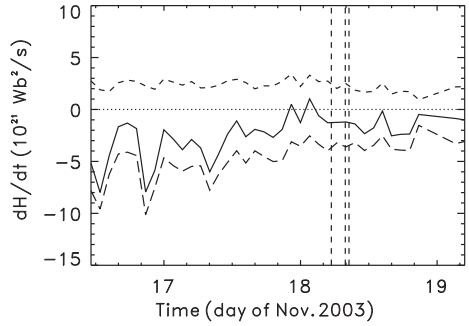

Fig. 6. Evolution of global magnetic helicity rate versus time in AR 10501. Short dashed line is the positive part, long dashed line is the negative part, continuous line is the total helicity. The vertical dashed lines are drawn at the times of the flares.

were injected in the AR. There is, therefore, enough magnetic helicity to generate a CME and a MC for which the average helicity is estimated to be about 10^{26} Wb^2 (DeVore, 2000; Lynch et al., 2005). Moreover, AR 10501 is a mature region; therefore, a much larger amount of helicity has probably been injected before. Most intense flaring ARs have a helicity larger than 10^{26} Wb^2 (LaBonte et al., 2007) with an average helicity for erupting regions of about 13×10^{26} Wb^2 (measured from the emergence of the AR, Nindos and Andrews, 2004).

However, the problem remains that the sign of the helicity accumulated in this AR is opposite to the helicity sign in the associated MC. Chandra et al. (2010) explained this contradiction computing the helicity flux maps of G_θ shown in Fig. 7 (see Pariat et al., 2005). These maps are computed using the line of sight magnetic field component and the flux transport velocity (Welsch, 2006) that corresponds to the motions of the magnetic structures at the photospheric surface. In this example, the velocity is computed using the method proposed by Schuck (2006). The global region has a negative helicity sign because the main spot remains of negative helicity sign during all its disk passage. However, in the left bottom panel, a strong shear appears between P4 and N4 where the filament is erupting and the helicity injection is mainly positive. This region involves a volume with loops connecting P4 to N4, according to the coronal magnetic extrapolation, with positive magnetic helicity. This agrees with a local magnetic helicity injection in this region. Then, we conclude that the MC, with positive helicity, was ejected from this portion of the AR, so solving the previous helicity sign paradox (Chandra et al., 2010).

4. Solar activity on 20 November 2003 and Magnetic cloud of 22 November 2003

4.1. Flares

On 20 November 2003, two homologous flares took place within around five hours in AR 10501, which was located approximately at N03 W05 at that time. The first flare (M1.4) presents a pre-flare phase at ≈01:30 UT. Its main phase started at 01:45 UT with a gradual onset,

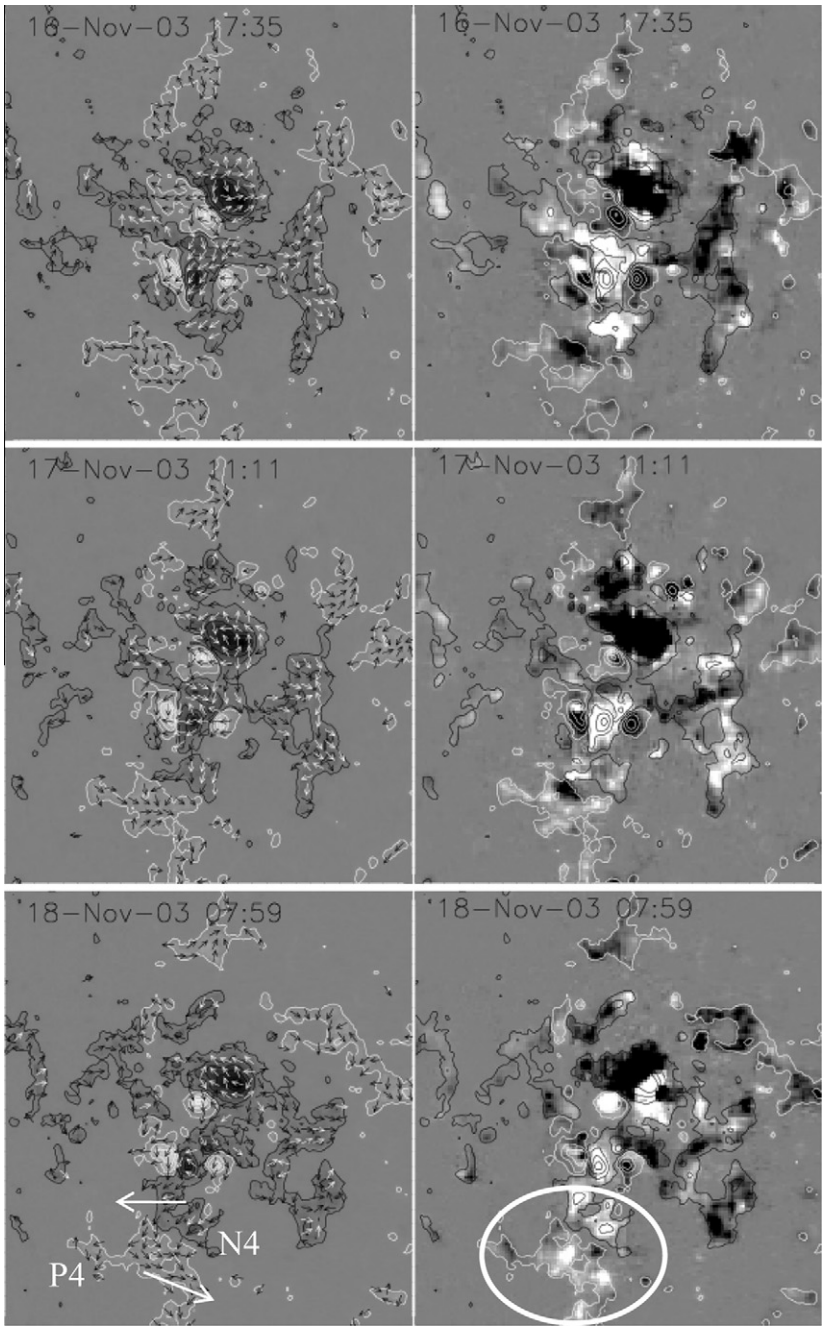

Fig. 7. Evolution of the magnetic field and magnetic helicity injection in AR 10501 on November 2003. The field-of-view is of $279'' \times 299'' = 202$ Mm $\times$ 217 Mm. (left panels) Longitudinal MDI magnetograms with flux transport velocity field u (arrows). (right panels) helicity flux density (G_θ) maps. Note that the saturation level, equal to 10^6 Wb^2 m^2 s^2, has been chosen to enhance the distribution of helicity in the magnetic polarities of intermediate intensity. The white (resp. black) continuous lines correspond to the + (resp. −) 100; 600; 1200; 1800 G isolevels of the longitudinal magnetic field distribution. The large white arrows in the low left panel indicate the shear between P4 and N4. adapted from Chandra et al. (2010)

peaked at 02:12 UT, and ended around 02:40 UT. As the flare evolved, two filaments located along two different magnetic inversion lines at the east of the AR were observed to approach each other, then they merged at their central parts and separated again forming a new configuration where they have interchanged their connections, just like field lines reconnecting. During all the interchange process the filaments remained stable and did not erupted. Török et al. (2011) explain the interaction of these filaments by a MHD simulation. The first flare was accompanied by a CME, which was rather slow ($\approx$364 km s^{-1}) and had a low projected angular width ($\approx 60^0$). This CME became visible in LASCO/C2 field-of-view at 02:48 UT (see http://cdaw.gsfc.nasa.gov/CMElist/.

The second flare started with a weak (C3.8) precursor at around 7:30 UT. Its main phase began with an impulsive

onset at 07:35 UT, it peaked at 07:45 UT and reached class M9.6. Finally, the flare ended gradually at around 09:00 UT. This flare was accompanied by the eruption of the filaments and by a full halo CME. This CME, which became visible in LASCO/C2 at 08:06 UT (Fig. 8), was faster ($\approx$670 km s^{-1}) than the first one. Though the flares were morphologically similar, the soft X-ray GOES light curve seems to indicate a more gradual energy release during the first flare than during the second one.

The peculiarity of this AR on 18 November 2003 was that it presented regions with different magnetic helicity signs (Section 3). This characteristic is also present on 20 November 2003 (Chandra et al., in press). Moreover, the magnetic configuration of the emerging flux P3N3 (Fig. 5) is getting fragmented. In particular, the polarity N3 separates in a few small polarities which rotate in a clockwise direction around P3 in a context of large dispersion of the main spots and of the network at the periphery. The flare initiation is forced by the continuous motion of the emerging bipole P3N3 (Kumar et al., 2010; Chandra et al., in press).

4.2. Interplanetary mass ejection

Fig. 9 shows *in situ* observations of the magnetic field on 22 November 2003 measured by ACE. At 10:00 UT we observe a shock with a strong increase of B, from 8 nT to 13 nT. After this high magnetic field structure, the magnetic field vector starts to rotate (11:45 UT), consistent with the observation of an interplanetary flux rope. The component B_y goes from values near zero to values larger than 5 nT (at $\sim$14:30 UT) and returns to near zero values at 18:00 UT. This evolution is characteristic of the axial field component present within a flux rope in MCs. The component B_z starts with a large value and globally decreases passing through zero, at a similar time B_y is maximum and then continues decreasing, becoming more negative, up to the strong discontinuity observed at 18:00 UT. Thus, the coherent rotation ends at 18:00 UT. This evolution is characteristic of the azimuthal field component within a flux rope.

One possible interpretation of these observations is that the plasma between 10:00 UT and 11:45 UT corresponds to the sheath, between the shock driven by an ICME and the flux rope behind (from 11:45 UT to 18:00 UT). The enhancement and rotation of the magnetic field is perhaps the signature of an interplanetary flux rope. In this case it is a NES rope (Bothmer and Schwenn, 1994, see right panel of Fig. 9) and its helicity is positive, which is again opposite to the helicity of the associated active region.

On the other hand, Gopalswamy et al. (2009) argued that a CME can be deflected towards the Sun-Earth line as well as away from it depending on the spatial location of the AR on the solar disk. In the case of the eruption on 20 November, they concluded that the coronal holes deflected the CME away from the Sun–Earth line and that only a shock and its following compressed region were observed on 22 November by the ACE spacecraft. Then, in this case, ACE observed only the lateral extension of the shocked region (which is typically more extended than the flux rope as shown by MHD simulations, e.g., Lugaz et al., 2005).

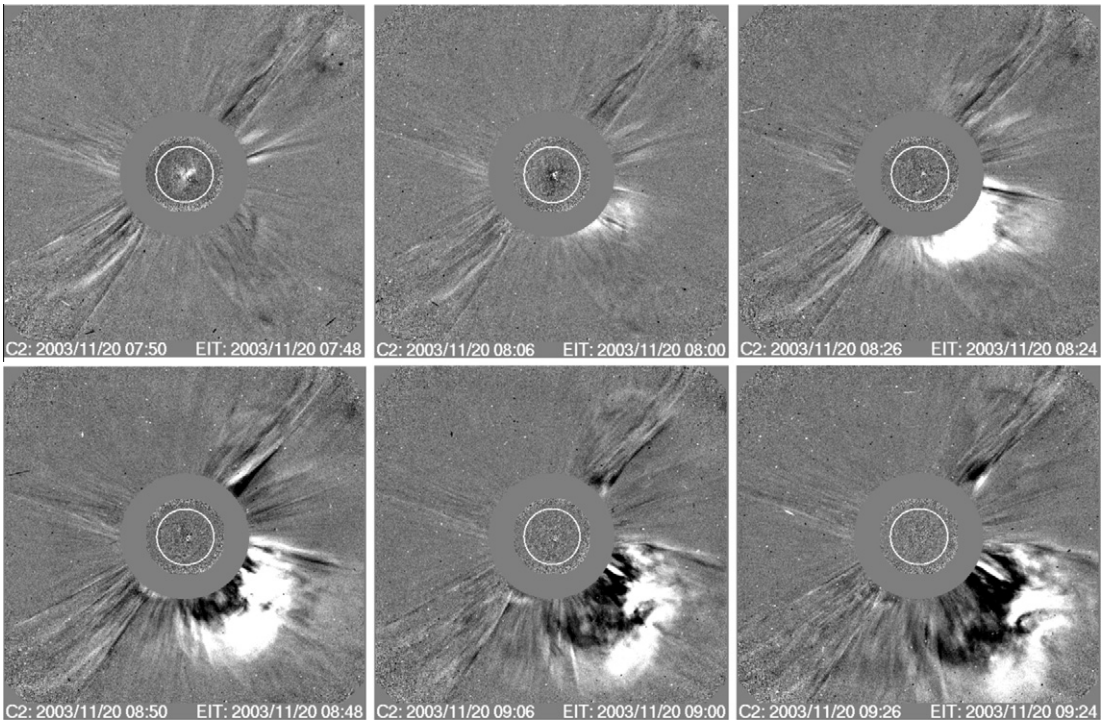

Fig. 8. Evolution of the CME observed on 20 November 2003 by LASCO/C2.

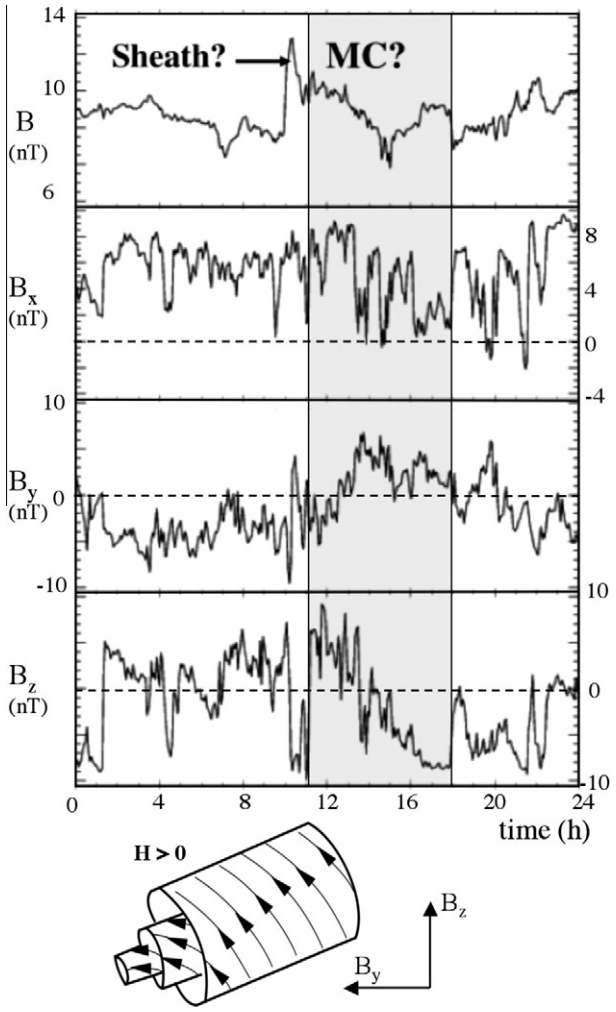

Fig. 9. (top panels) *In situ* observations on 22 November 2003 of the magnetic field by ACE, with from the upper to the lower panel, the magnetic field strength (B) and the components (B_x, B_y, and B_z) of the magnetic field vector in the GSE system of coordinates. (bottom panel) Sketch of the orientation and the helicity of the flux rope as deduced from the *in situ* observations.

Indeed, both views could be compatible since, while the azimuthal field component of the flux rope is well present in the B_z component, the axial field component is weak in the B_y component (and a rotation of the coordinate system would not change this difference). This indicates that the spacecraft crossed the flux rope far from its axis as the axial field component typically decreases away from the axis. This is confirmed by a strong B_x component, also indicating an large impact parameter (Gulisano et al., 2007). Then ACE probably observed only the lateral side of the flux rope, where it is typically strongly distorted by its interaction with the solar wind.

5. Evolution of the ICME from scintillation measurements

The ICME has also been traced out in the inner heliosphere using interplanetary scintillation (IPS) observations made at the Ooty Radio Telescope on a large number of radio sources (e.g., Manoharan, 2006). The inner heliosphere is reconstructed in 3D through the use of the University of California, San Diego (UCSD), reconstruction program incorporating a time dependent kinematic solar wind model (Jackson et al., 2003; Jackson et al., in press). IPS LOS weighting distribution depends on the different observed frequencies and source sizes. This weighting factor is a result of the IPS response to the Fresnel filtering effect (Coles and Harmon, 1978) and to radio source size, as described in Jackson et al. (1998). The tomographic reconstruction provides the velocity and normalized density ($n_{norm} = nr^2$) structures associated with the expansion of the ICME in a 3-AU diameter heliosphere.

Fig. 10 displays the tomography reconstruction of the heliospheric structure obtained from the IPS measurements at Ooty (e.g., Jackson et al., in press; Manoharan, 2010). These images shows the normalized density and velocity of the solar wind as seen in the ecliptic plane on 20 November 2003 at 6 UT. The enhanced density corresponds to the

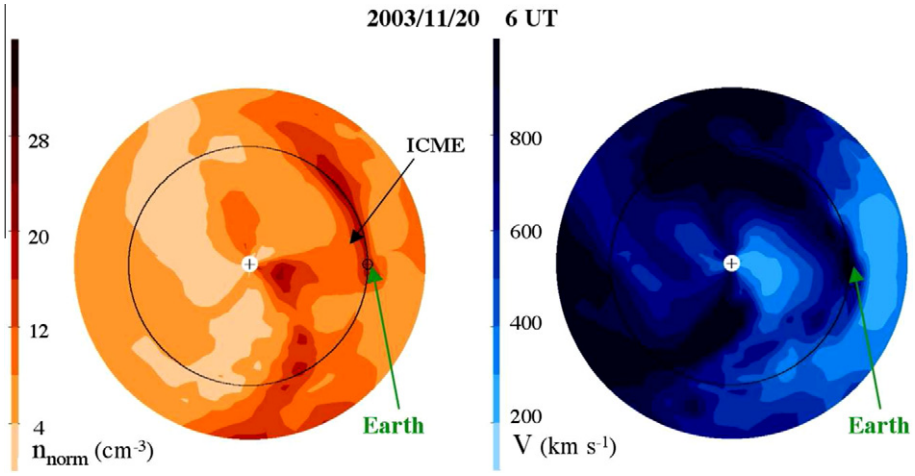

Fig. 10. Images of normalized plasma density ($n_{norm} = nr^2$) and velocity in the interplanetary space showing the front of the ICME overtaking Earth, as derived from Ooty IPS observations on 20 November 2003 at 6 UT. In these images Sun is at the center and they show the ecliptic view of the heliosphere of diameter 3 AU. These images are reconstructed using the program developed at UCSD (e.g., Jackson et al., in press; Manoharan, 2010).

time and location of the ICME and its associated magnetic cloud near the orbit of the Earth. A long extended dense structure is crossing Earth's orbit in the ecliptic plane. Close to the Earth, the density enhancement could correspond to the sheath in front of the CME, away of the Earth the elongated density structure could correspond to a co-rotating interaction region (CIR). The velocity increases from 400 to 700–800 km/s as the cloud is crossing the Earth. This is consistent with the enhancement in the velocity detected by ACE as the sheath is observed (Fig. 3).

The radial progression of a dense region on November 22 is shown in an eastward direction from the Earth (Fig. 11a and c) with an outward gradient of velocity (Fig. 11b and d). There is also another dense region, moving westward and away from Earth, which is not related to the above studied ICME. As expected, the observed structures on the 23 November are mainly the ones observed one day earlier with an outward drift.

However, the results in the ecliptic plane provide only a very partial view of the studied ICME since it was passing mostly northward from Earth. Fig. 11e,f show the 3D results on 23 November with two points of view. A very elongated excess of density is present mainly above the ecliptic plane. We associate this enhanced density to the

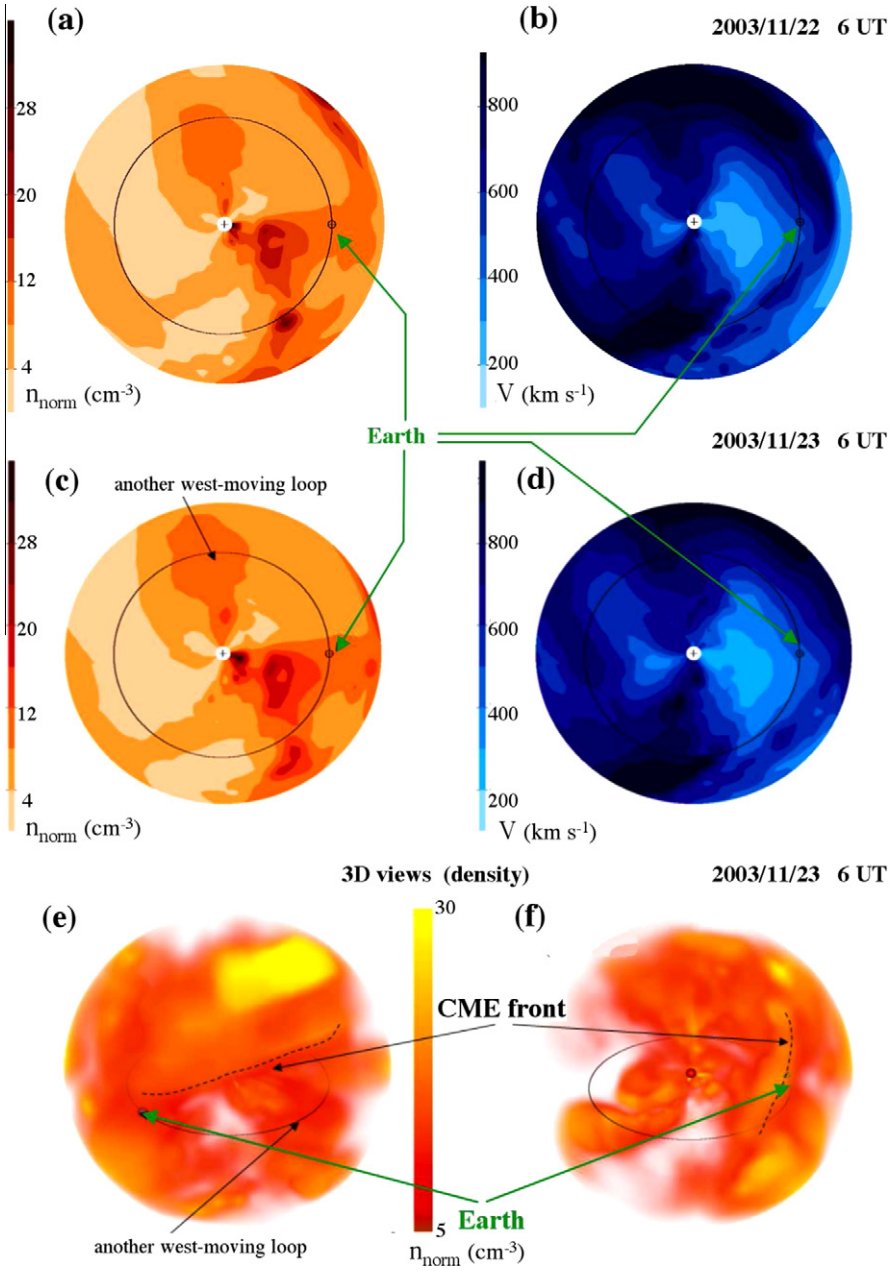

Fig. 11. Images of normalized density ($n_{norm} = nr^2$) and velocity of the solar wind showing the front of the ICME derived from Ooty IPS observations in the ecliptic plane on 22 (top panels) and 23 November 2003 (middle panels; also refer to Fig. 2 and Kumar et al., 2010). The bottom row is the remote view the heliosphere of size 3 AU, as seen 30 degree above the ecliptic plane. In the above images Sun is at the center and they have been obtained by using the reconstruction program developed at UCSD (e.g., Jackson et al., in press; Manoharan, 2010).

sheath present in front of the flux rope located within the ICME. According to these observations the enhanced density structure, and therefore also the flux rope behind it, is inclined by about 50° on the ecliptic plane (Kumar et al., 2010). Its north foot is above the ecliptic plane, the south foot is below. This is approximately consistent with the orientation of the flux rope deduced from *in situ* observations (Fig. 9). The 3D results also show that the main part of the ICME was passing significantly northward to Earth, and ACE. This is consistent with the weak flux rope signatures obtained from *in situ* observations as the impact parameter is large (Section 4.2).

6. Conclusion

In this study, we describe the activity in AR NOAA 10501 on 18 and 20 November 2003. We show that the main actor in this large and complex active region is the emergence of new magnetic flux which induces shearing and stress in the magnetic field. This consequently drives a large scale instability of the magnetic configuration leading to flares, filament eruptions, CMEs, and ICMEs. A comparison of *in situ* measurements by ACE and IPS data shows the complementarity of these observations. The association of the ICME observed by ACE and IPS enhancement of density is very clear for the event of 20 November 2003. On 22 November 2003 the observation of ACE shows a weak signature of MC due to the orientation of the cloud in respect of ACE direction, however in the three dimensional reconstruction of IPS data a clear ICME structure is evidenced.

Acknowledgments

The authors thank CEFIPRA Project 3704-1 for its support to this study on "Transient events in Sun Earth System" during our bilateral collaboration. Some of the authors thank ISSI in Bern where this work has been deeply analyzed and discussed in the workshop chaired by Consuelo Cid. BS, PD, EP thank the European network "SOLAIRE" for fruitful discussions with a few network team members. T.T. is supported by the NASA HTP and LWS programs.The authors acknowledge financial support from ECOS-Sud through their cooperative science program (N^o A08U01). CHM acknowledges financial support from the Argentinean grants UBACyT X127, PIP 2009-100766 (CONICET), and PICT 1790 (ANPCyT). S.D. thanks the Argentinean grants UBACyT 20020090100264 and PICT 00856 (ANPCyT). SD and CHM are members of the Carrera del Investigador Científico, CONICET. We also thank the two referees for their comments, which help us to clarify the paper.

References

Berger, M.A. Rigorous new limits on magnetic helicity dissipation in the solar corona. Geophys. Astrophys. Fluid Dyn. 30, 79–104, 1984.

Bisi, M.M., Breen, A.R., Jackson, B.V., Fallows, R.A., Walsh, A.P., Mikić, Z., Riley, P., Owen, C.J., Gonzalez-Esparza, A., Aguilar-Rodriguez, E., Morgan, H., Jensen, E.A., Wood, A.G., Owens, M.J., Tokumaru, M., Manoharan, P.K., Chashei, I.V., Giunta, A.S., Linker, J.A., Shishov, V.I., Tyul'Bashev, S.A., Agalya, G., Glubokova, S.K., Hamilton, M.S., Fujiki, K., Hick, P.P., Clover, J.M., Pintér, B. From the sun to the earth: The 13 may 2005 coronal mass ejection. Solar Phys. 265, 49–127, 2010a.

Bisi, M.M., Jackson, B.V., Breen, A.R., Dorrian, G.D., Fallows, R.A., Clover, J.M., Hick, P.P. Three-dimensional (3-d) reconstructions of EISCAT IPS velocity data in the declining phase of solar cycle 23. Solar Phys. 265, 233–244, 2010b.

Bothmer, V., Schwenn, R. Eruptive prominences as sources of magnetic clouds in the solar wind. Space Sci. Rev. 70, 215–220, 1994.

Brueckner, G.E., Howard, R.A., Koomen, M.J., Korendyke, C.M., Michels, D.J., Moses, J.D., Socker, D.G., Dere, K.P., Lamy, P.L., Llebaria, A., Bout, M.V., Schwenn, R., Simnett, G.M., Bedford, D.K., Eyles, C.J. The large angle spectroscopic coronagraph (LASCO). Solar Phys. 162, 357–402, 1995.

Burlaga, L., Sittler, E., Mariani, F., Schwenn, R. Magnetic loop behind an interplanetary shock – voyager, Helios, and IMP 8 observations. J. Geophys. Res. 86, 6673–6684, 1981.

Chandra, R., Pariat, E., Schmieder, B., Mandrini, C.H., Uddin, W. How can a negative magnetic helicity active region generate a positive helicity magnetic cloud? Solar Phys. 261, 127–148, 2010.

Chandra, R., Schmieder, B., Aulanier, G., Malherbe, J.M. Evidence of magnetic helicity in emerging flux and associated flare. Solar Phys. 258, 53–67, 2009.

Chandra, R., Schmieder, B., Mandrini, C., Démoulin, P., Pariat, E., Török, T., Uddin, W. Homologous Flares and Magnetic Field Topology in Active Region NOAA 10501 on 20 November 2003, Solar Phys., in press, doi:10.1007/s11207-010-9670-9.

Coles, W.A., Harmon, J.K. Interplanetary scintillation measurements of the electron density power spectrum in the solar wind. J. Geophys. Res. 83, 1413–1420, 1978.

Dasso, S., Mandrini, C.H., Démoulin, P., Luoni, M.L. A new model-independent method to compute magnetic helicity in magnetic clouds. Astron. Astrophys. 455, 349–359, 2006.

Dasso, S., Mandrini, C.H., Schmieder, B., Cremades, H., Cid, C., Cerrato, Y., Saiz, E., Démoulin, P., Zhukov, A.N., Rodriguez, L., Aran, A., Menvielle, M., Poedts, S. Linking two consecutive nonmerging magnetic clouds with their solar sources. J. Geophys. Res. 114, A02109, 2009.

Dasso, S., Nakwacki, M.S., Démoulin, P., Mandrini, C.H. Progressive transformation of a flux rope to an ICME. Comparative analysis using the direct and fitted expansion methods. Solar Phys. 244, 115–137, 2007.

Démoulin, P. A review of the quantitative links between CMEs and magnetic clouds. Ann. Geophys. 26, 3113–3125, 2008.

Démoulin, P., Pariat, E. Modelling and observations of photospheric magnetic helicity. Adv. Space Res. 43, 1013–1031, 2009.

DeVore, C.R. Magnetic helicity generation by solar differential rotation. Astrophys. J. 539, 944–953, 2000.

Fan, Y., Gibson, S.E. The emergence of a twisted magnetic flux tube into a preexisting coronal arcade. Astrophys. J. Lett. 589, L105–L108, 2003.

Gopalswamy, N., Lara, A., Lepping, R.P., Kaiser, M.L., Berdichevsky, D., St. Cyr, O.C. Interplanetary acceleration of coronal mass ejections. Geophys. Res. Lett. 27, 145–148, 2000.

Gopalswamy, N., Mäkelä, P., Xie, H., Akiyama, S., Yashiro, S. CME interactions with coronal holes and their interplanetary consequences. J. Geophys. Res. 114, A00A22, 2009.

Gopalswamy, N., Xie, H., Mäkelä, P., Akiyama, S., Yashiro, S., Kaiser, M.L., Howard, R.A., Bougeret, J. Interplanetary shocks lacking type II radio bursts. Astrophys. J. 710, 1111–1126, 2010.

Gopalswamy, N., Yashiro, S., Michalek, G., Xie, H., Lepping, R.P., Howard, R.A. Solar source of the largest geomagnetic storm of cycle 23. Geophys. Res. Lett. 32, 12, 2005.

Green, L.M., Kliem, B., Török, T., van Driel-Gesztelyi, L., Attrill, G.D.R. Transient coronal sigmoids and rotating erupting flux ropes. Solar Phys. 246, 365–391, 2007.

Gulisano, A.M., Dasso, S., Mandrini, C.H., Démoulin, P. Estimation of the bias of the minimum variance technique in the determination of magnetic clouds global quantities and orientation. Adv. Space Res. 40, 1881–1890, 2007.

Hoang, S., Lacombe, C., MacDowall, R.J., Thejappa, G. Radio tracking of the interplanetary coronal mass ejection driven shock crossed by Ulysses on 10 May 2001. J. Geophys. Res. 112 (A11), A09102, 2007.

Jackson, B.V., Hick, P.L., Kojima, M., Yokobe, A. Heliospheric tomography using interplanetary scintillation observations 1. Combined Nagoya and Cambridge data. J. Geophys. Res. 103, 12049–12068, 1998.

Jackson, B.V., Hick, P.P., Buffington, A., Bisi, M.M., Clover, J.M., Tokumaru, M., Kojima, M., Fujiki, K. Three-dimensional reconstruction of heliospheric structure using iterative tomography: a review, J. Atmos. Sol. Terr. Phys., in press, doi:10.1016/j.jastp.2010.10.007.

Jackson, B.V., Hick, P.P., Buffington, A., Kojima, M., Tokumaru, M., Fujiki, K., Ohmi, T., Yamashita, M. Time-dependent tomography of hemispheric features using interplanetary scintillation (IPS) remote-sensing observations, in: Solar Wind Ten., American Institute of Physics Conference Series, Vol. 679, pp. 75–78, 2003.

Kumar, P., Manoharan, P.K., Uddin, W. Evolution of solar magnetic field and associated multiwavelength phenomena: Flare events on 2003 november 20. Astrophys. J. 710, 1195–1204, 2010.

LaBonte, B.J., Georgoulis, M.K., Rust, D.M. Survey of magnetic helicity injection in regions producing X-class flares. Astrophys. J. 671, 955–963, 2007.

López Fuentes, M.C., Démoulin, P., Mandrini, C.H., van Driel-Gesztelyi, L. The counterkink rotation of a non-hale active region. Astrophys. J. 544, 540–549, 2000.

Lugaz, N., Manchester IV, W.B., Gombosi, T.I. The evolution of coronal mass ejection density structures. Astrophys. J. 627, 1019–1030, 2005.

Lynch, B.J., Gruesbeck, J.R., Zurbuchen, T.H., Antiochos, S.K. Solar cycle-dependent helicity transport by magnetic clouds. J. Geophys. Res. 110 (A9), A08107, 2005.

Mandrini, C.H., Démoulin, P., Schmieder, B., Deluca, E.E., Pariat, E., Uddin, W. Companion event and precursor of the X17 flare on 28 October 2003. Solar Phys. 238, 293–312, 2006.

Manoharan, P.K. Evolution of coronal mass ejections in the inner heliosphere: A study using white-light and scintillation images. Solar Phys. 235, 345–368, 2006.

Manoharan, P.K. Ooty interplanetary scintillation – remote-sensing observations and analysis of coronal mass ejections in the heliosphere. Solar Phys. 265, 137–157, 2010.

Marubashi, K. Interplanetary magnetic flux ropes and solar filaments in coronal mass ejections. Geophys. Monograph 99, 147–156, 1997.

Möstl, C., Miklenic, C., Farrugia, C.J., Temmer, M., Veronig, A., Galvin, A.B., Vrsnak, B., Biernat, H.K. Two-spacecraft reconstruction of a magnetic cloud and comparison to its solar source. Ann. Geophys. 26, 3139–3152, 2008.

Nindos, A., Andrews, M.D. The association of big flares and coronal mass ejections: What is the role of magnetic helicity? Astrophys. J. Lett. 616, L175–L178, 2004.

Pariat, E., Démoulin, P., Berger, M.A. Photospheric flux density of magnetic helicity. Astron. Astrophys. 439, 1191–1203, 2005.

Park, S.-H., Lee, J., Choe, G.S., Chae, J., Jeong, H., Yang, G., Jing, J., Wang, H. The variation of relative magnetic helicity around major flares. Astrophys. J. 686, 1397–1403, 2008.

Schmieder, B., Mandrini, C.H., Démoulin, P., Pariat, E., Berlicki, A., Deluca, E. Magnetic reconfiguration before the X 17 solar flare of October 28 2003. Adv. Space Res. 37, 1313–1316, 2006.

Schuck, P.W. Tracking magnetic footpoints with the magnetic induction equation. Astrophys. J. 646, 1358–1391, 2006.

Smith, C.W., L'Heureux, J., Ness, N.F., Acuña, M.H., Burlaga, L.F., Scheifele, J. The ACE magnetic fields experiment. Space Sci. Rev. 86, 613–632, 1998.

Srivastava, N., Mathew, S.K., Louis, R.E., Wiegelmann, T. Source region of the 18 November 2003 coronal mass ejection that led to the strongest magnetic storm of cycle 23. J. Geophys. Res. (Space Phys.) 114, A03107, 2009.

St. Cyr, O.C., Howard, R.A., Sheeley, N.R., Plunkett, S.P., Michels, D.J., Paswaters, S.E., Koomen, M.J., Simnett, G.M., Thompson, B.J., Gurman, J.B., Schwenn, R., Webb, D.F., Hildner, E., Lamy, P.L. Properties of coronal mass ejections: SOHO LASCO observations from January 1996 to June 1998. J. Geophys. Res. 105, 18169–18185, 2000.

Stone, E.C., Frandsen, A.M., Mewaldt, R.A., Christian, E.R., Margolies, D., Ormes, J.F., Snow, F. The advanced composition explorer. Space Sci. Rev. 86, 1–22, 1998.

Török, T., Chandra, R., Pariat, E., Démoulin, P., Schmieder, B., Aulanier, G., Linton, M.G., Mandrini, C.H. Filament interaction modeled by flux rope reconnection. Astrophys. J. 728, 65, 2011.

Török, T., Kliem, B. Confined and ejective eruptions of kink-unstable flux ropes. Astrophys. J. Lett. 630, L97–L100, 2005.

Wang, Y., Zhou, G., Ye, P., Wang, S., Wang, J. A study of the orientation of interplanetary magnetic clouds and solar filaments. Astrophys. J. 651, 1245–1255, 2006.

Watari, S., Watanabe, T., Marubashi, K. Soft X-ray solar activities associated with interplanetary magnetic flux ropes. Solar Phys. 202, 363–384, 2001.

Welsch, B.T. Magnetic flux cancellation and coronal magnetic energy. Astrophys. J. 638, 1101–1109, 2006.

Williams, D.R., Török, T., Démoulin, P., van Driel-Gesztelyi, L., Kliem, B. Eruption of a kink-unstable filament in NOAA active region 10696. Astrophys. J. Lett. 628, L163–L166, 2005.

Yurchyshyn, V., Hu, Q., Abramenko, V. Structure of magnetic fields in NOAA active regions 0486 and 0501 and in the associated interplanetary ejecta. Space Weather 3, S08C02, 2005.

Yurchyshyn, V., Liu, C., Abramenko, V., Krall, J. The May 13, 2005 eruption: Observations, data analysis and interpretation. Solar Phys. 239, 317–335, 2006.

Yurchyshyn, V.B., Wang, H., Goode, P.R., Deng, Y. Orientation of the magnetic fields in interplanetary flux ropes and solar filaments. Astrophys. J. 563, 381–388, 2001.

Zhukov, A.N., Veselovsky, I.S. Global coronal mass ejections. Astrophys. J. Lett. 664, L131–L134, 2007.